SCIENTIFIC REPORTS

OPEN

Ferroelectric Metal in Tetragonal $BiCoO_3/BiFeO_3$ Bilayers and Its Electric Field Effect

Received: 21 September 2015
Accepted: 07 January 2016
Published: 03 February 2016

Li Yin[1], Wenbo Mi[1] & Xiaocha Wang[2]

By first-principles calculations we investigate the electronic structure of tetragonal $BiCoO_3/BiFeO_3$ bilayers with different terminations. The multiferroic insulator $BiCoO_3$ and $BiFeO_3$ transform into metal in all of three models. Particularly, energetically favored model CoO_2-BiO exhibits ferroelectric metallic properties, and external electric field enhances the ferroelectric displacements significantly. The metallic character is mainly associated to e_g electrons, while t_{2g} electrons are responsible for ferroelectric properties. Moreover, the strong hybridization between e_g and O *p* electrons around Fermi level provides conditions to the coexistence of ferroelectric and metallic properties. These special behaviors of electrons are influenced by the interfacial electronic reconstruction with formed Bi-O electrovalent bond, which breaks O_A-Fe/Co-O_B coupling partially. Besides, the external electric field reverses spin polarization of Fe/Co ions efficiently, even reaching 100%.

Multiferroics with ferroelectricity, ferromagnetism or ferroelasticity simultaneously have great potential applications in information storage, electronic devices and sensors[1–3]. Particularly, magneto-electric multiferroics, where the spontaneous ferroelectric polarization can be controlled by an external magnetic field or vice versa, are found in perovskite-type transition metal oxides providing bright prospect for novel spintronic devices[4–8]. Oxide heterostructures exhibit unique properties absent in the corresponding isolated parent compounds, therefore it is an effective means to study emergent physics of correlated electrons, such as, metal-insulator transition[9], two-dimensional electron gas and sharp interfaces at $LaAlO_3/SrTiO_3$ interfaces[10–13], orientation-dependent magnetism and so on[14]. Besides, recent technology advances in oxide synthesis at the atomic level make artificially designing heterostructures feasible[15]. We attempt to combine two perovskite-like multiferroics into bilayers aimed at inducing novel electronic and magnetic states, providing theoretical support for new multifunction devices as well. We pay attention upon Bi-based perovskite materials, whose ferroelectric properties originates from a lone pair of $(6s)^2$ electrons[16–18], and select tetragonal $BiFeO_3$ (BFO) and $BiCoO_3$ (BCO) as multiferroics candidates.

The perovskite BFO is the only known room-temperature single-phase magneto-electric multiferroic material, which is intensively studied in the last decade, with a high ferroelectric Curie temperature of 1103 K and antiferromagnetic Neel temperature of 643 K[19–23], exhibiting weak magnetism at room temperature due to a residual moment from a canted spin structure[24]. Notablely, tetragonal BFO has much higher spontaneous polarization of 150 $\mu C/cm^2$ and charge transfer excitations than rhombohedral phase, and gets considerable high resistance changes in ferroelectric tunnel junctions[25–29]. The resistance changes in ferroelectric tunnel junctions based on tetragonal BFO are considerably high (OFF/ON ratio >10000) among known ferroelectric tunnel junctions[30]. BCO has been suggested to be a promising multiferroic material, which is predicted to exhibit a giant polarization and extremely high transition temperature[31,32]. The ferroelectricity of BCO is found to be primarily driven by the lone-pair activity of Bi^{3+}, and magnetism being driven by the high-spin state of Co^{3+} in a C-type antiferromagnetic structure below a Neel temperature of 420 K[33,34]. And, BFO and BCO with large spontaneous ferroelectric polarization have great potential application in electrically controllable devices[35–39]. Besides, compounding BFO with BCO is accessible experimentally in the form of epitaxial thin film[40] and the BFO/BCO multiferroic solid solutions are studied theoretically[41]. Previous studies show that the antiferromagnetic insulator $BiFeO_3$ can exhibit ferromagnetism in $BiFeO_3/La_{2/3}Sr_{1/3}MnO_3$ interface[42,43] and two-dimensional electron gas in $BiFeO_3/SrTiO_3$ interface[44], demonstrating that heterointerface is significant in $BiFeO_3$-based bilayers. However,

[1]Tianjin Key Laboratory of Low Dimensional Materials Physics and Preparation Technology, Faculty of Science, Tianjin University, Tianjin, 300072, China. [2]Tianjin Key Laboratory of Film Electronic & Communicate Devices, School of Electronics Information Engineering, Tianjin University of Technology, Tianjin, 300384, China. Correspondence and requests for materials should be addressed to W.M. (email: miwenbo@tju.edu.cn)

the heterostructures by constructing $BiFeO_3$ with another multiferroic $BiCoO_3$ may present some fantastic properties based on its multiferroic characteristics.

In this paper, we study the electronic structure of BCO/BFO bilayers with different terminations and investigate the external electric field effect on the bilayers by first-principles calculations. We find that energetically favored model CoO_2-BiO exhibits ferroelectric metallic properties due to the division of e_g and t_{2g} electrons as well as e_g-p hybridization. Additional, external electric field enhances the ferroelectric displacements markedly. These special behaviors of electrons are influenced by the interfacial electronic reconstruction with formed Bi-O electrovalent bond, which breaks O_A-Fe/Co-O_B coupling partially. Our results indicate that interfacial coupling and electric field play key roles on the novel ferroelectric metallic properties of model CoO_2-BiO, which provides opportunities for developing functional nanoelectronic devices.

Calculation Details

Our first-principle calculations are performed using density functional theory (DFT) within the local spin-density approximation (LSDA), based on the projector augment wave (PAW) pseudo-potentials. The energy cutoff for plane wave basis set is 500 eV and the Brillouin zone is sampled with Γ-centered $5 \times 5 \times 5$ and $5 \times 5 \times 1$ k point meshes for bulk compounds and bilayers respectively, providing numerical convergence of 10^{-5} eV. All the structures are fully relaxed until the maximum Hellmann-Feynman forces on each atom are less than 0.02 eV/Å. Aimed at getting reasonable results, we include an on-site Coulomb repulsion of $U = 6$ eV for Co 3d states[45], and $U = 4.5$ eV for Fe 3d states[46,47], which are sufficient to describe the related bulk properties.

Tetragonal phase of the multiferroic BFO used in this work has a perovskite-type structure with a lattice constant of $a = 3.770$ Å and $c/a = 1.233$ in space group $P4mm$[47]. The primitive cell of tetragonal BFO contains one molecule with one Bi atom located at (0.0, 0.0, 0.0), one Fe atom at (0.5, 0.5, 0.439), one axial O_A atom at (0.5, 0.5, −0.170) in BiO layer and two equatorial O_B atoms at (0.0, 0.5, 0.294) and (0.5, 0.0, 0.294) in FeO_2 layer. The magnetic character of BFO is G-type where the Fe atoms are coupled ferromagnetically within the (111) planes and antiferromagnetically between adjacent planes. Bulk BCO is an antiferromagnetic insulator of C-type which is the most stable magnetic order in BCO[48], where Co ions are aligned antiferromagnetically in the xy plane and ferromagnetically along the z axis, with a lattice constant of $a = 3.729$ Å and $c/a = 1.267$ in space group $P4mm$[45]. The used experiment value of atomic coordinates in BCO are Bi (0.0, 0.0, 0.0), Co (0.5, 0.5, 0.5669), one axial O_A (0.5, 0.5, 0.2034) and two equatorial O_B (0.5, 0.0, 0.73)[33]. Bi ions locate in the corner sites, yet Fe (or Co) ions and O ions which ought to occupy the body and face centered sites respectively move from center sites in the z direction owing to ferroelectric spontaneous polarization. In the supercells of BCO/BFO studied here, a 28 Å vacuum space in z direction is used to separate the interaction between periodic images and the supercells are built by placing five BCO atomic layers on the top of five BFO atomic layers within $p(\sqrt{2} \times \sqrt{2})$ periodicity giving altering layers of Bi_2O_2 and Co_2O_4 (Fe_2O_4) along the [001] direction. In experiments, the thin films must present one surface that is exposed in the vacuum, even though the sample is a multilayered structure. Hence, the bilayer geometry with vacuum should be calculated. Meanwhile, the difference of optimized geometry and atomic position can affect the multiferroics of the sample. In superlattice structure, there are two interfaces which might influence the relaxation of the atoms, so that each atomic position should be different from the case of bilayer with vacuum. Meanwhile, in order to study the effect of external electric field, the bilayer with vacuum is necessary. We apply external electric field for the bilayers in z direction and switch on the potential correction mode. The calculated in-plane lattice mismatch between BFO(001) and BCO(001) is 1.1%, indicating a good lattice match. We set up three BCO/BFO bilayers with different terminations to investigate the interfacial properties, as shown in Fig. 1(a–c).

The stable pattern is determined by calculating the work of separation, i.e., the cohesive energy between BCO and BFO, $W_{sep} = E_{BCO} + E_{BFO} - E_{BCO/BFO}$, where $E_{BCO/BFO}$ is the total energy of the bilayers, E_{BCO} and E_{BFO} represent the energies of the same supercell containing either the BCO or BFO parts (i.e., we keep the equilibrium structure obtained for the bilayers). For illustrating the nature of the charge transfer at BCO/BFO interface, we calculate the charge density difference by subtracting the charge densities of isolated BFO and BCO parts from the charge density of bilayers as shown in Fig. 1(d–l). The electronic structures of isolated BFO and BCO are calculated by freezing the atoms of the respective component at the supercell positions.

Results and Discussion

First, we analyze the total and projected densities of states (DOS) of fully relaxed bulk BFO and BCO shown in Fig. 2. For BFO, the charge transfer gap is determined by the filled oxygen 2p band and the unoccupied 3d band of Fe, and the calculated band gap of 1.93 eV is in good agreement with previous calculations[49], but inconsistent with the experimental value of 3.10 eV[50], as a result of using the LSDA approximation. The Fe spins are antiparallel and the corresponding DOS is symmetrical, so we only show one. The calculated Fe magnetic moments are ± 4.107 μ_B per atom. For BCO, the calculated total DOS is similar with previous calculations[45], and the Co ions are in high-spin state which is consistent with the experimental result[33], as shown in Fig. 2(a,d). The spin-up and spin-down band structures are completely compatible, so we only show spin-up structure in Fig. 2(e). We find that the strong correlated effect of Co 3d is well described with a band gap of 1.52 eV and the Co magnetic moments are ± 3.035 μ_B per atom, which are in good agreement with the experimental values of 1.7 eV and 3.24 μ_B[33,51]. These bulk results reveal that the used parameters in the present work are reasonable.

We carry out the electronic band structures of three models and separate out the BCO's contribution to demonstrate the changes of the electronic states in BCO by comparing with bulk BCO states in same path, as shown in Fig. 3. Obviously, both BCO and BFO transforms into metal in all of three interfacial models and BCO undergoes a dramatic change, revealing that interfacial compound probably is an efficient method to explore emergent physics as well. The strong interfacial effect is also reflected by the remarkable accumulation and depletion of electrons at interfaces, as shown in Fig. 1(d–l). Bi and O ions combine with each other in the form of electrovalent bond with Bi depleting and O accumulating electrons in the interfacial regions of model CoO_2-BiO

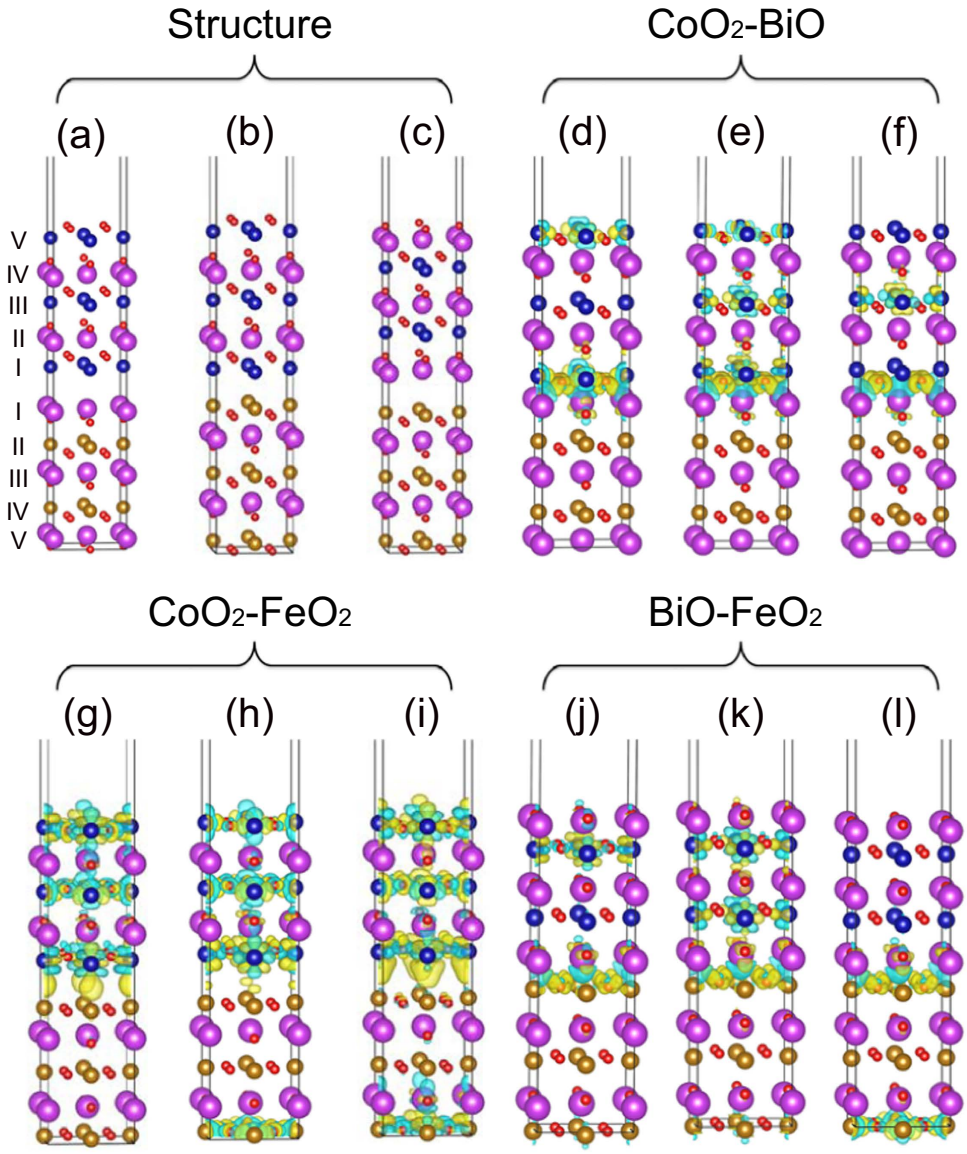

Figure 1. (**a–c**) side views of BCO/BFO bilayers for model CoO_2-BiO, CoO_2-FeO_2 and BiO-FeO_2 respectively. (**d–f**) charge density difference of model CoO_2-BiO (isosurface value 0.008 e/Å^3) in $E = 0$, 6 and 10 mV/Å respectively, (**g–i**) for model CoO_2-FeO_2 (isosurface value 0.003 e/Å^3)and (**j–l**) for model BiO-FeO_2 (isosurface value 0.008 e/Å^3). The red spheres stand for O, dark yellow for Fe, dark blue for Co and purple for Bi. The yellow and blue isosurfaces represent accumulation and depletion of electrons, respectively.

and BiO-FeO_2, see Fig. 2(d,j). For model CoO_2-FeO_2, apparent accumulation of electrons between Co and Fe occurs at the interfacial regions revealing that Co and Fe ions combine via metallic bond we propose, as shown in Fig. 2(g). The calculated cohesive energies demonstrate that model CoO_2-BiO is the most stable structure with a considerably large value of 11.474 eV and model CoO_2-FeO_2 is very unstable with a negative value, as listed in Table 1, which is reasonable since the interfaces in model CoO_2-BiO and BiO-FeO_2 are similar with the structures of bulk BCO and BFO, while model CoO_2-FeO_2 totally not.

We further analyze the geometric structure of three models and the Bi-O, Fe-O and Co-O polar displacements of three models in one layer along [001] direction are calculated by subtracting the position of O ions. The black lines in Fig. 4 indicate that the displacements of model CoO_2-BiO is larger than the other two models and we list the average values in Table 1. It is obvious that the displacements in model CoO_2-BiO is almost 50% larger than model CoO_2-FeO_2 and model BiO-FeO_2 and nearly three quarters of correspond bulks. Therefore, model CoO_2-BiO exhibit metallic properties with remarkable ferroelectric structures since tetragonal BCO and BFO are typical displacive ferroelectrics originating from relative displacement of positive and negative ions[27,48,52,53]. To further investigate its ferroelectric properties, we add an electric field to all of three bilayers considering the strong electric field effect on ferroelectrics owing to the spontaneous polarization. Based on the experimental study on bulk[52,54], we add the electric field of 6 and 10 mV/Å (i.e., 600 and 1000 kV/cm) respectively and calculated the relative displacements of positive and negative ions in same layer along z axis, as shown in Fig. 4. We find that

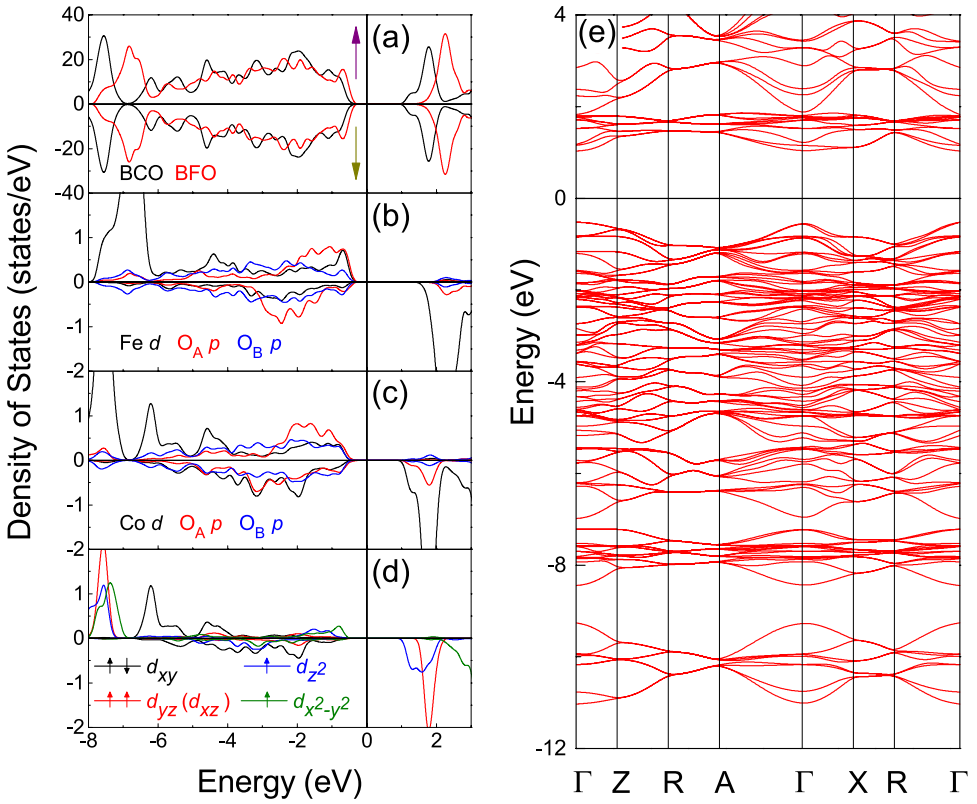

Figure 2. (**a**) Total DOS for bulk BFO and BCO. (**b**) Partial DOS for bulk BFO. (**c**) Partial DOS for bulk BCO. (**d**) DOS for Co *d* electrons in bulk BCO. The Fermi level is indicated by vertical lines and set to zero. (**e**) Spin-up band structure of bulk BCO.

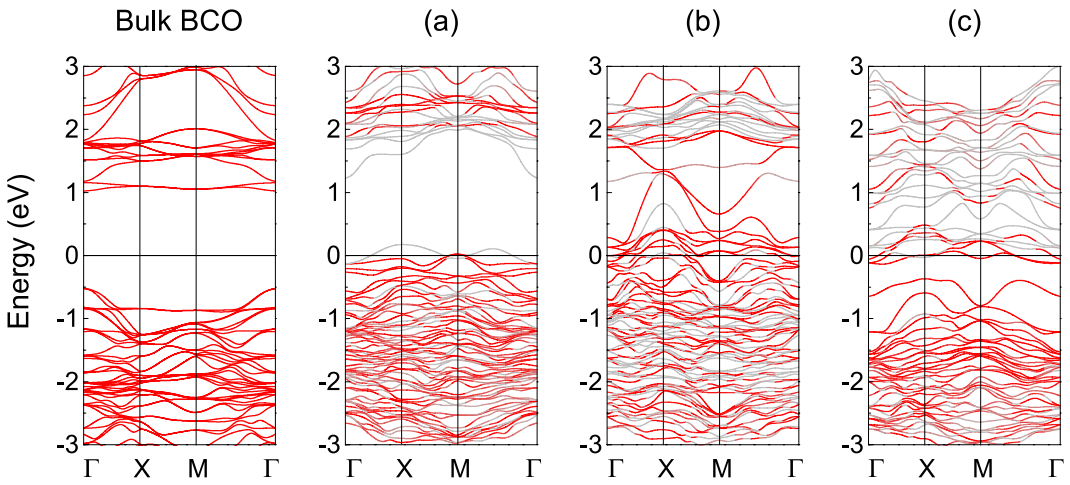

Figure 3. Spin-up band structure of bulk BCO, model (**a**) CoO_2-BiO, (**b**) CoO_2-FeO_2 and (**c**) BiO-FeO_2 bilayers. The red color indicates BCO and gray BFO. $E_F = 0$ eV.

the polarization displacements in model CoO_2-FeO_2 and model BiO-FeO_2 with electric field (see red and blue lines) are close to the situation without electric field (see black lines) shown in Fig. 4(b,c), but the polarization shifts in model CoO_2-BiO are enhanced greatly on the condition of applied electric field, particularly at the interfacial regions as shown in Fig. 4(a). This result further confirms the ferroelectric metallic properties of model CoO_2-BiO and demonstrates that external electric field can modulate the ferroelectric polarization. Figure 1(d) reveals the strong interfacial coupling by Bi-O electrovalent bonds in the interfacial regions of model CoO_2-BiO, and we further notice that the interfacial Bi-O bonds exist even in applied electric field, as shown in Fig. 1(e,f). This short-range pair interaction makes the ferroelectric polarization properties of bulks preserved in bilayers and lowers the electrostatic energy further stabilize the bilayers structure.

	Bulk	CoO_2-BiO (mV/Å)			CoO_2-FeO_2 (mV/Å)			BiO-FeO_2 (mV/Å)		
		$E=0$	$E=6$	$E=10$	$E=0$	$E=6$	$E=10$	$E=0$	$E=6$	$E=10$
$d_{Bi\text{-}O}$	0.803	0.582	0.654	0.646	0.268	0.248	0.273	0.364	0.403	0.365
$d_{B\text{-}O}$	0.643	0.402	0.485	0.455	0.167	0.147	0.188	0.172	0.227	0.157
W_{sep}	–	11.474	12.378	11.754	−1.998	−3.150	−2.886	6.442	8.900	7.626

Table 1. The average values of Bi-O and B-O polar displacements in one layer along [001] direction in three models within different values of external electric field, B = Co/Fe. Corresponding cohesive energy *Wsep* is listed.

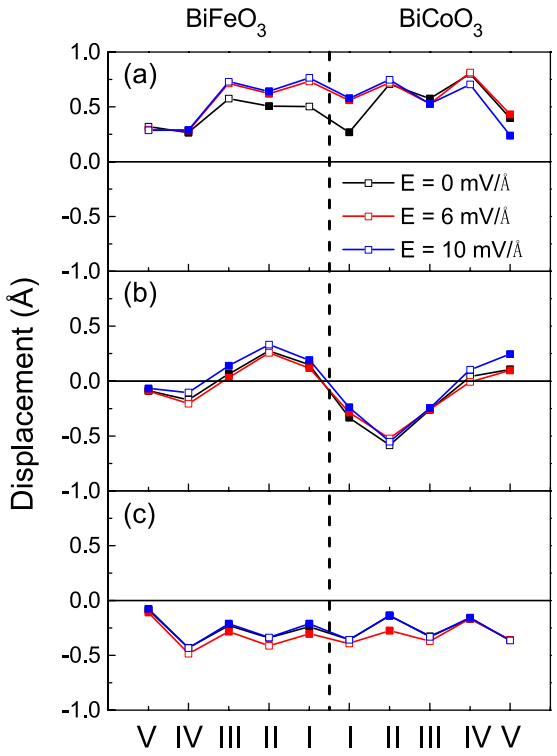

Figure 4. The change of Bi-O and B-O polar displacements in each layer along [001] direction in model (**a**) CoO_2-BiO, (**b**) CoO_2-FeO_2 and (**c**) BiO-FeO_2 due to different values of external electric field, B = Co/Fe. Open square symbols represent Bi-O displacements, and solid square symbols represent B-O displacements.

On the other hand, the structure of models CoO_2-BiO and BiO-FeO_2 contains two asymmetry surfaces and might be as polar as $LaAlO_3/SrTiO_3$ interface within a large "internal" electric field[9,55], which automatically gives rise to the metallicity of the system. We check the same asymmetry geometry in pure BFO and BCO, which possesses the form $(BiO\text{-}MO_2)_n$ within 15 Å vacuum space in *z* direction (M = Fe/Co, n = 2, 3, 4). The calculated band structures indicate that such pure BFO is insulating when n = 2/3 but exhibits metallic in $n = 4$, while the pure BCO is metallic and not affected by *n*. Hence, the asymmetry structure is important for the metallic characters in CoO_2-BiO model. Furthermore, such pure metallic properties in BFO and BCO are distinguished from the metallic characters in model CoO_2-BiO. Firstly, both uppermost valence band (UVB) and lowest conduction band (LCB) approach the Fermi level in $(BiO\text{-}FeO_2)_4$, while the LCB of isolated BFO in model CoO_2-BiO is far away from the Fermi level (see Fig. 3a). Secondly, the UVB in pure BCO overlaps with the Fermi level heavily, while the UVB of isolated $BiCoO_3$ in CoO_2-BiO model only approach the Fermi level (see Fig. 3a). It is obvious that the strong interfacial couplings have a great effect on the metallic characters in CoO_2-BiO model.

Next, we analyze the electronic DOS distribution of ions in the interfacial regions of model CoO_2-BiO in detail shown in Fig. 5. We find that, for BCO, I-Co *d* electrons hybridize with II-O *p* electrons distinctly but interact weakly with I-O *p* electrons in the energy range from −3 eV to Fermi level (E_F) as indicated in Fig. 5(a). Similarly, for BFO, II-Fe *d* electrons hybridize obviously with II-O *p* electrons while lightly with I-O *p* electrons in the energy window from −1.2 to −0.3 eV as shown in Fig. 5(b). The label "I-Co" represents the Co ions in layer I as shown in Fig. 1(a), and this kind of definition is used in the whole letter. For bulk BCO and BFO, Fe/Co ions hybridize with O_A and O_B, along with clear O alignment as shown in Fig. 2(b,c). For model CoO_2-BiO, the interfacial Bi-O bonds make I-O *p* electrons in BFO and BCO change dramatically and break the balance of O_A-Fe/Co-O_B partially, which further influences the metallic properties of bilayers with retained ferroelectric properties.

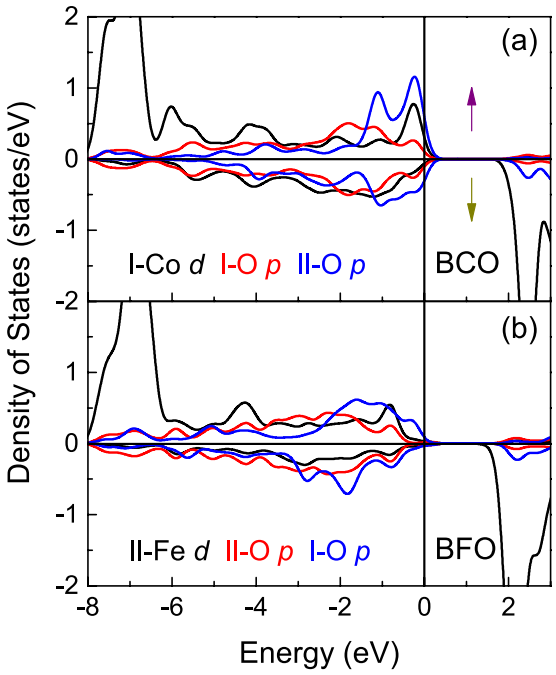

Figure 5. DOS for Fe, Co and O ions in interfacial regions of model CoO_2-BiO. $E_F = 0$ eV.

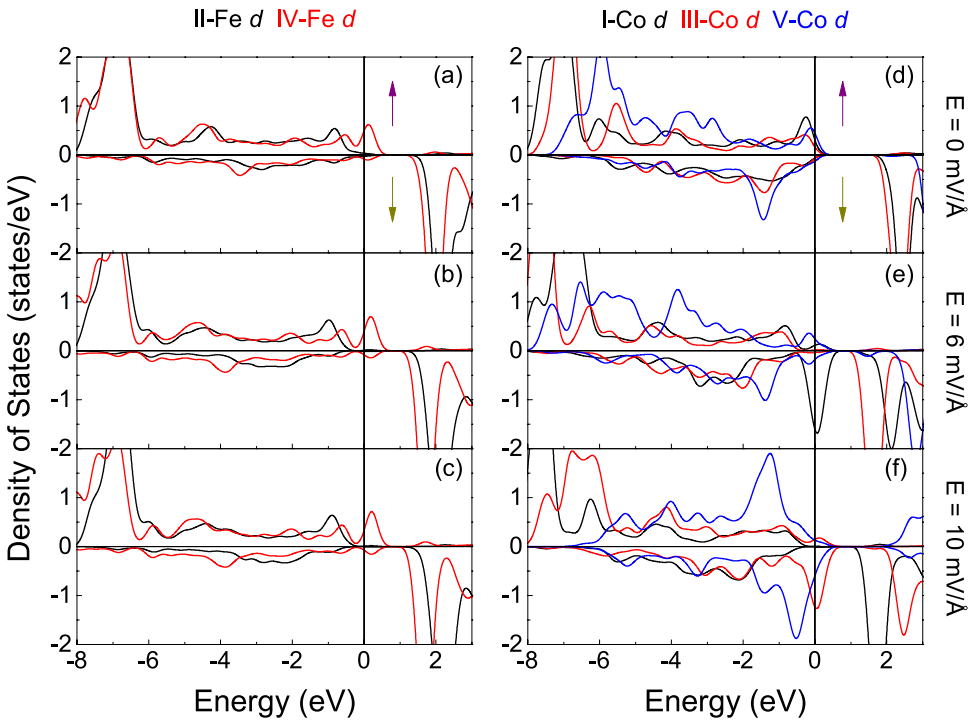

Figure 6. Partial DOS for (**a**–**c**) Fe and (**d**–**f**) Co in each layer of model CoO_2-BiO on different values of electric field. $E_F = 0$ eV.

Then, we analyze the Fe/Co DOS in each layer in different on the condition of electric field or not, as shown in Fig. 6. The Fe electronic distribution varies gently as indicated by Fig. 6(a–c), while Co ions change heavily shown in Fig. 6(d–f). We define spin polarization $P = (N_{\uparrow}(E_F) - N_{\downarrow}(E_F))/(N_{\uparrow}(E_F) + N_{\downarrow}(E_F))$ in terms of the total DOS in the spin-up $N_{\uparrow}$ and spin-down $N_{\downarrow}$ channels respectively, and find that the spin polarization of I-Co is reversed from 70% to −89% on the condition of $E = 6$ mV/Å by comparing Fig. 6(d) with Fig. 6(e). Besides, the spin polarization of III-Co and V-Co are reversed from 49% to −82% and 54% to −62% respectively on the condition of

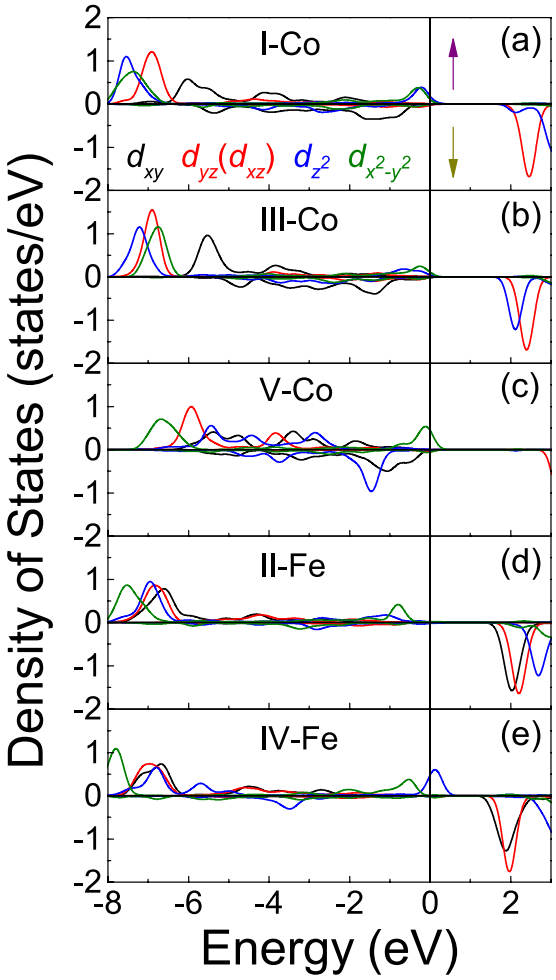

Figure 7. DOS for Co/Fe *d* electrons in each layer of model CoO_2-BiO. $E_F = 0$ eV.

Atom		Bulk	CoO_2-BiO (mV/Å)			CoO_2-FeO_2 (mV/Å)			BiO-FeO_2 (mV/Å)		
			$E=0$	$E=6$	$E=10$	$E=0$	$E=6$	$E=10$	$E=0$	$E=6$	$E=10$
Co	I	3.035	3.009	2.902	3.046	2.898	2.516	0.889	–	–	–
	II		–	–	–	–	–	–	1.829	3.067	1.809
	III		3.032	3.040	2.808	2.633	2.575	2.696	–	–	–
	IV		–	–	–	–	–	–	1.698	2.972	2.988
	V		2.624	2.642	1.052	2.017	3.016	2.228	–	–	–
Fe	I	4.108	–	–	–	3.936	3.910	3.969	4.120	4.099	4.125
	II		4.076	4.093	4.090	–	–	–	–	–	–
	III		–	–	–	3.624	3.644	3.741	4.084	4.092	4.096
	IV		3.765	3.605	3.573	–	–	–	–	–	–
	V		–	–	–	3.841	2.797	1.695	4.010	3.968	2.861
Total		0.000	0.000	0.000	0.000	0.000	0.000	0.000	0.000	0.000	0.000

Table 2. The calculated magnetic moments (μ_B) of Fe and Co in each layer of three models as compared to the bulk.

$E = 10$ mV/Å according to Fig. 6(d,f). The apparent positive-negative spin polarization reverse in Co ions demonstrates that electric field not only can be used to induce magnetic moments via magneto-electric effect as previous report[2], but also can reverse spin polarization. The Fe/Co magnetic moments are listed in Table 2, which are influenced heavily by interfacial effect and electric field. The numbers of Fe/Co magnetic moments in same layer are equal but with different signs, so we only list the positive numbers in Table 2. In addition, the Co magnetic moments are changed easily, which is reasonable since the Co ions possess flexible possibilities of high, intermediate and low spin states. The electronic rearrangements of Co caused by interfacial coupling are also reflected by

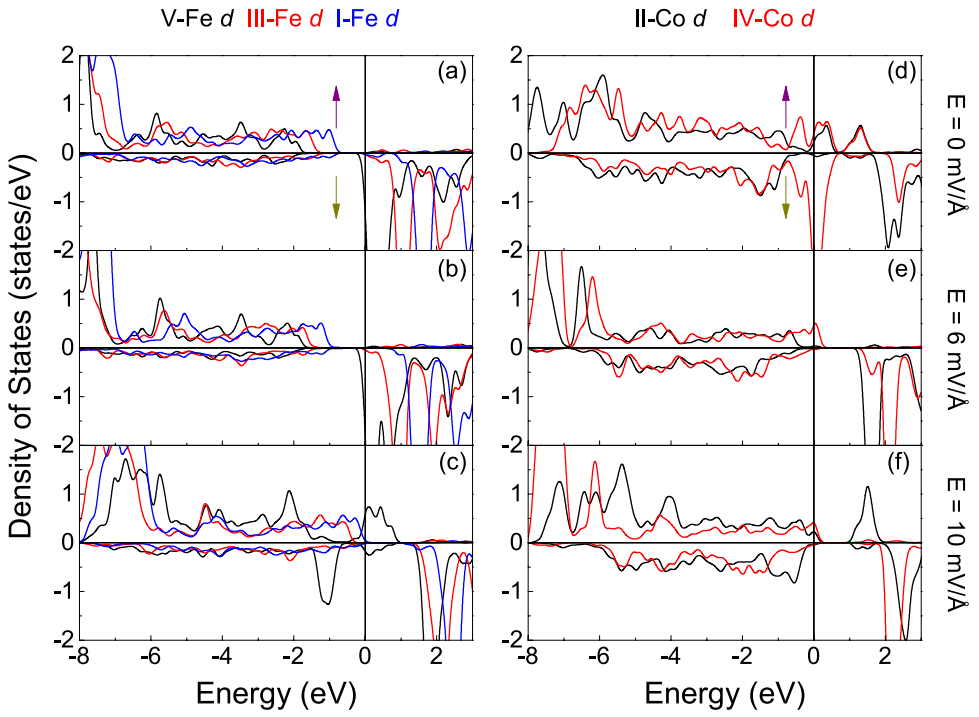

Figure 8. Partial DOS for (**a**–**c**) Fe and (**d**–**f**) Co in each layer of model BiO-FeO_2 on different values of electric field. $E_F = 0$ eV.

charge density difference since electrons with different orbital contours increase or decrease, shown in Fig. 1(d–l).

Although it is widely believed that metals cannot exhibit ferroelectricity since the static internal electric fields are screened by conduction electrons[56], the ferroelectric metal is theoretically proposed by Anderson and Blount in 1965[57]. Recently $LiOsO_3$ is identified as the first typical example[58], and the microscopic mechanism for the ferroelectric-like structural transition in a metal are investigate widely[59,60]. The Mott multiferroic based on $LiOsO_3$ is predicted by compounding with $LiNbO_3$ as well[61]. However, in our model CoO_2-BiO, the ferroelectrics are transformed into metal from insulator via interfacial coupling, which is opposite the $LiOsO_3$-type metal into ferroelectric transition. The itinerant *d* electrons can screen the electric fields and inhibit the electrostatic forces, so we analyze the *d* electron states of Fe/Co ions in each layer of model CoO_2-BiO on purpose as shown in Fig. 7. We find that the metallic property is associated to the electrons in e_g orbitals (i.e., d_{z^2} and $d_{x^2-y^2}$), and these electrons hybridize with O *p* electrons around E_F according to Fig. 5. However, the electrons in t_{2g} orbitals (i.e., d_{xy}, d_{xz}, and d_{yz}) have no contribution to the metallic character, which are responsible for the ferroelectric properties as shown in Figs 2(d) and 7. Therefore, although the specific e_g electrons exhibit metallic property, they simultaneously hybridize with O *p* electrons, which makes ferroelectric and metallic features coexist. And we argue that this special electron occupation is tightly associated with the interfacial coupling as mentioned above.

On the other hand, the ferroelectric displacements are not sensitive to external electric field in model BiO-FeO_2 as shown in Fig. 4(c), and we believe that the different behavior of models CoO_2-BiO and BiO-FeO_2 is a result of termination effect. It is also found in model BiO-FeO_2 that the electric field reverses spin polarization of Fe/Co ions. Figure 8(d–f) indicate that the spin polarization of IV-Co are reversed from −73% to 100% upon $E = 6$ and 10 mV/Å, While V-Fe are reversed from −100% to 53% upon $E = 10$ mV/Å according to Fig. 8(a,c). These results show that electric field can not only reverse the positive and negative of spin polarization, but also reach a considerable value even 100%. In addition, the synthesis technology of oxides has beem improved significantly, such as MBE MOCVD, etc., which can fabricate high-quality epitaxial films and heterostructures. We take the $La_{0.7}Sr_{0.3}MnO_3/BiFeO_3$ structures as an example. For the growth of $La_{0.7}Sr_{0.3}O$ terminated $La_{0.7}Sr_{0.3}MnO_3$ film, Yu *et al.* modify the $SrTiO_3$ substrate from TiO_2 termination to SrO termination[62]. To achieve this, a very thin layer (2.5 unit cells) of $SrRuO_3$ was grown on $SrTiO_3$, or growing one monolayer of SrO on the TiO_2 terminated $SrTiO_3$ substrate. And Kim *et al.* also fabricated the $BiFeO_3$-MnO_2-terminated and $BiFeO_3$-(La,Sr)O-terminated $La_{0.7}Sr_{0.3}MnO_3$ structures in similar method[63]. Therefore, the energetically unfavored termination can be achieved by inserting specific monolayer in the stable termination. The prediction of ferroelectric metallic characteristics in $BiFeO_3/BiCoO_3$ bilayers is meaningful for the expertimental research, which can provide opportunities for developing novel functional electronic devices.

Conclusion

In summary, we investigate the electronic structure of BCO/BFO(001) bilayers with different terminations based on first-principles calculations. The multiferroic insulator BCO and BFO transform into metal in all of three

models. Particularly, energetically favored model CoO_2-BiO exhibits ferroelectric metallic properties and external electric field enhances the ferroelectric displacements markedly. The metallic character is mainly associated to the e_g electrons of Fe/Co ions and these electrons simultaneously hybridize with O p electrons around E_F, yet the t_{2g} electrons are responsible for ferroelectric properties. Therefore, the division of e_g and t_{2g} electrons as well as e_g-p hybridization provide conditions to the coexistence of ferroelectric and metallic properties. These special behaviors of electrons are influenced by the interfacial electronic reconstruction with formed Bi-O electrovalent bond, which breaks O_A-Fe/Co-O_B coupling partially. Besides, strong interfacial coupling changes the Fe/Co magnetic moments and external electric field reverses spin polarization of Fe/Co ions efficiently, reaching a maximum of 100%. Our results demonstrate that interfacial coupling and electric field play key roles on the novel ferroelectric metallic properties of model CoO_2-BiO, which provides opportunities for developing functional nanoelectronic devices. We hope that our theoretical prediction on the ferroelectric metallic properties and corresponding electric field effect can stimulate further experimental study.

References

1. Ramesh, R. & Spaldin, N. A. Multiferroics: progress and prospects in thin films. *Nat. Mater.* **6,** 21–9 (2007).
2. Tokura, Y. Multiferroics as quantum electromagnets. *Science* **312,** 1481–1482 (2006).
3. Fiebig, M. Revival of the magnetoelectric effect. *J. Phys. D* **38,** R123–R148 (2005).
4. Gibert, M., Zubko, P., Scherwitzl, R. Iniguez, J. & Triscone, J. M. Exchange bias in $LaNiO_3$-$LaMnO_3$ superlattices. *Nat. Mater.* **11,** 195–198 (2012).
5. Hur, N. *et al.* Electric polarization reversal and memory in a multiferroic material induced by magnetic fields. *Nature* **429,** 389–392 (2004).
6. Eerenstein, W., Mathur, N. D. & Scott, J. F. Multiferroic and magnetoelectric materials. *Nature* (London) **442,** 759–65 (2006).
7. Spaldin, N. A. & Fiebig, M. The renaissance of magnetoelectric multiferroics. *Science* **309,** 391–392 (2005).
8. Cheong, S. W. & Mostovoy, M. Multiferroics: a magnetic twist for ferroelectricity. *Nat. Mater*. **6,** 13–20 (2007).
9. Ohtomo, A. & Hwang, H. Y. A high-mobility electron gas at the $LaAlO_3$/$SrTiO_3$ heterointerface. *Nature* **427,** 423–426 (2004).
10. Cossu, F., Jilili, J. & Schwingenschlögl, U. 2D electron gas with 100% spin-polarization in the $(LaMnO_3)_2$/$(SrTiO_3)_2$ superlattice under uniaxial strain. *Adv. Mater.* **1,** 1400057 (2014).
11. Jeong, H. Y. & Lee, J. H. Critical thickness for the two-dimensional electron gas in $LaTiO_3$/$SrTiO_3$ superlattice. *Phys. Rev. B* **88,** 155111 (2013).
12. Zhang, Z., Wu, P., Chen, L. & Wang, J. L. First-principles prediction of a two dimensional electron gas at the $BiFeO_3$/$SrTiO_3$ interface. *Appl. Phys. Lett.* **99,** 062902 (2011).
13. Nakagawa, N., Hwang, H. Y. & Muller, D. A. Why some interfaces cannot be sharp. *Nat. Mater.* **5,** 204–209 (2006).
14. Dong, S. & Dagotto, E. Quantum confinement induced magnetism in LaNiO3-$LaMnO_3$ superlattice. *Phys. Rev. B* **87,** 195116 (2013).
15. Hwang, H. Y. *et al.* Emergent phenomena at oxide interfaces. *Nat. Mater.* **11,** 103–113(2012).
16. Cohen, R. E. Origin of ferroelectricity in perovskite oxides. *Nature* **358,** 136–138 (1992).
17. Baettig, P., Schelle, C. F., LeSar, R., Waghmare, U. V. & Spaldin, N. A. Theoretical prediction of new high-performance lead-free piezoelectrics. *Chem. Mater.* **17,** 1376–1380 (2005).
18. Iniguez, J., Vanderbilt, D. & Bellaiche, L. First-principles study of $(BiScO_3)_{1-x}$-$(PbTiO_3)_x$ piezoelectric alloys. *Phys. Rev. B* **67,** 224107 (2003).
19. Catalan, G. & Scott, J. F. Physics and applications of bismuth ferrite. *Adv. Mater.* **21,** 2463–2485 (2009).
20. Kiselev, S. V., Ozerov, R. P. & Zhdanov, G. S. Detection of magnetic order in ferroelectric $BiFeO_3$ by neutron diffraction. *Sov. Phys. Dokl.* **7,** 742–744 (1963).
21. Neaton, J. B., Ederer, C., Waghmare, U. V., Spaldin, N. A. & Rabe, K. M. First-principles study of spontaneous polarization in multiferroic $BiFeO_3$. *Phys. Rev. B* **71,** 014113 (2005).
22. Ederer, C. & Spaldin, N. A. Weak ferromagnetism and magnetoelectric coupling in bismuth ferrit. *Phys. Rev. B* **71,** 060401R (2005).
23. Lebeugle, D. *et al.* Electric-field-induced spin flop in $BiFeO_3$ single crystals at room temperature. *Phys. Rev. Lett.* **100,** 227602 (2008).
24. Smolenskii, G. A. & Chupis, I. Ferroelectromagnets. *Sov. Phys. Usp.* **25,** 475–493 (1982).
25. Zeches, R. J. *et al.* A strain-driven morphotropic phase boundary in $BiFeO_3$. *Science* **326,** 977–80 (2009).
26. Damodaran, A. R. *et al.* Nanoscale structure and mechanism for enhanced electromechanical response of highly strained $BiFeO_3$ thin films. *Adv. Mater.* **23,** 3170–3175 (2011).
27. Hatt, A. J., Spaldin, N. A. & Ederer, C. Strain-induced isosymmetric phase transition in $BiFeO_3$. *Phys. Rev. B* **81,** 054109 (2010).
28. Martin, L. W. *et al.* Multiferroics and magnetoelectrics: thin films and nanostructures. *J. Phys. Condens. Matter* **20,** 434220 (2008).
29. Chen, P. *et al.* Optical properties of quasi-tetragonal $BiFeO_3$ thin films. *Appl. Phys. Lett.* **96,** 131907 (2010).
30. Yamada, H. *et al.* Giant electroresistance of super-tetragonal $BiFeO_3$-based ferroelectric tunnel junctions. *ACS Nano* **7,** 5385–5390 (2013).
31. Yoshitaka, U., Tatsuya, S., Fumiyuki, I. & Tamio, O. First-principles predictions of giant electric polarization. *Jpn. J. Appl. Phys.* **44,** 7130–7133 (2005).
32. Oka, K. *et al.* Magnetic ground-state of perovskite $PbVO_3$ with large tetragonal distortion. *Inorg. Chem.* **47,** 7355–7359 (2008).
33. Belik, A. A. *et al.* Neutron powder diffraction study on the crystal and magnetic structures of $BiCoO_3$. *Chem. Mater.* **18,** 798–803 (2006).
34. Das, T. & Saha-Dasgupta, T. Spin-state transition in unstrained and strained ultra-thin $BiCoO_3$ films. *Dalton Trans.* **44,** 10882–10887 (2015).
35. Wang, J. *et al.* Epitaxial $BiFeO_3$ multiferroic thin film heterostructures. *Science* **299,** 1719–1722 (2003).
36. Wang, J. *et al.* Response to comment on "epitaxial BiFeO3 multiferroic thin film heterostructures". *Science* **307,** 1203b (2005).
37. Bea, H. *et al.* Investigation on the origin of the magnetic moment of $BiFeO_3$ thin films by advanced x-ray characterizations. *Phys. Rev. B* **74,** 020101R (2006).
38. Bea, H. *et al.* Influence of parasitic phases on the properties of $BiFeO_3$ epitaxial thin films. *Appl. Phys. Lett.* **87,** 072508 (2005).
39. Rana, D. S. *et al.* Thickness dependence of the structure and magnetization of $BiFeO_3$ thin films on $(LaAlO_3)_{0.3}(Sr_2AlTaO_6)_{0.7}$ (001) substrate. *Phys. Rev. B* **75,** 060405R (2007).
40. Shintaro, Y. *et al.* Crystal structure and electrical properties of {100} oriented epitaxial $BiCoO_3$-$BiFeO_3$ films grown by metalorganic chemical vapor deposition. *Jpn. J. Appl. Phys.* **47,** 7582 (2008).
41. Dieguez, O. & Iniguez, J. First-principles investigation of morphotropic transitions and phase-change functional responses in $BiFeO_3$-$BiCoO_3$ multiferroic solid solutions. *Phys. Rev. Lett.* **107,** 057601 (2011).
42. Yu, P. *et al.* Interface ferromagnetism and orbital reconstruction in $BiFeO_3$-$La_{0.7}Sr_{0.3}MnO_3$ heterostructures. *Phys. Rev. Lett.* **105,** 027201 (2010).
43. Wu, S. M. *et al.* Reversible electric control of exchange bias in a multiferroic field-effect device. *Nat. Mater.* **9,** 756–761 (2010).
44. Chen, C. L. *et al.* Two-dimensional electron gas at the Ti-diffused $BiFeO_3$/$SrTiO_3$ interface. *Appl. Phys. Lett.* **107,** 031601 (2015).

45. Cai, M. Q. *et al.* First-principles study of structural, electronic, and multiferroic properties in $BiCoO_3$. *J. Chem. Phys.* **126,** 154708 (2007).
46. Feng, N., Mi, W. B., Wang, X. C. & Bai, H. L. The magnetism of Fe_4N/oxides (MgO, $BaTiO_3$, $BiFeO_3$) interfaces from first-principles calculations. *RSC Adv.* **4,** 48848 (2014).
47. Ricinschi, D., Yun, K. Y. & Okuyama, M. A mechanism for the 150 $\mu C\ cm^{-2}$ polarization of $BiFeO_3$ films based on first-principles calculations and new structural data. *J. Phys. Condens. Matter* **18,** L97–L105 (2006).
48. Sudayama, T. *et al.* Co-O-O-Co superexchange pathways enhanced by small charge-transfer energy in multiferroic $BiCoO_3$. *Phys. Rev. B* **83,** 235105 (2011).
49. Yang, H., Jin, C., Mi, W. B., Bai, H. L. & Chen, G. F. Electronic and magnetic structure of Fe_3O_4/$BiFeO_3$ multiferroic superlattices: first principles calculations. *J. Appl. Phys.* **112,** 063925 (2012).
50. Himcinschi, C. *et al.* Optical properties of epitaxial $BiFeO_3$ thin films grown on $LaAlO_3$. *Appl. Phys. Lett.* **106,** 012908 (2015).
51. McLeod, J. A. *et al.* Electronic structure of BiMO_3 multiferroics and related oxides. *Phys. Rev. B* **81,** 144103 (2010).
52. Zhang, J. X. *et al.* Microscopic origin of the giant ferroelectric polarization in tetragonal-like $BiFeO_3$. *Phys. Rev. Lett.* **107,** 147602 (2011).
53. Jia, T. *et al.* Ab initio study of the giant ferroelectric distortion and pressure-induced spin-state transition in $BiCoO_3$. *Phys. Rev. B* **83,** 174433 (2011).
54. Yun, K. Y., Ricinschi, D., Kanashima, T., Noda, M. & Okuyama, M. Giant ferroelectric polarization beyond 150 $\mu C/cm^2$ in $BiFeO_3$ thin film. *Jpn. J. Appl. Phys.* **43,** L647 (2004).
55. Weston, L., Cui, X. Y., Ringer, S. P. & Stampfl, C. Density-functional prediction of a surface magnetic phase in $SrTiO_3$/$LaAlO_3$ heterostructures induced by Al vacancies. *Phys. Rev. Lett.* **113,** 186401 (2014).
56. Lines, M. E. & Glass, A. M. *Principles and applications of ferroelectrics and related materials*. Oxford Univ. Press (2001).
57. Anderson, P. W. & Blount, E. I. Symmetry considerations on martensitic transformations: "ferroelectric" metals? *Phys. Rev. Lett.* **14,** 217–219 (1965).
58. Shi, Y. *et al.* A ferroelectric-like structural transition in a metal. *Nature Mater.* **12,** 1024–7 (2013).
59. Giovannetti, G. & Capone, M. Dual nature of the ferroelectric and metallic state in$LiOsO_3$. *Phys. Rev. B* **90,** 195113 (2014).
60. Xiang, H. J. Origin of polar distortion in $LiNbO_3$-type "ferroelectric" metals: role of *A*-site instability and short-range interactions. *Phys. Rev. B* **90,** 094108 (2014).
61. Puggioni, D., Giovannetti, G., Capone, M. & Rondinelli, J. M. Design of a Mott multiferroic from a nonmagnetic polar metal. *Phys. Rev. Lett.* **115,** 087202 (2015).
62. Yu, P. *et al.* Interface control of bulk ferroelectric polarization. *PNAS* **109,** 9710–9715 (2012).
63. Kim, Y. M. *et al.* Interplay of octahedral tilts and polar order in $BiFeO_3$ films. *Adv. Mater.* **25,** 2497–2504 (2013).
64. Kimura, T. *et al.* Magnetic control of ferroelectric polarization. *Nature* **426,** 55–58 (2003).

Acknowledgements

This work is supported by the National Natural Science Foundation of China (51171126, 11434006), Program for New Century Excellent Talents in University (NCET-13-0409). It is also supported by High Performance Computing Center of Tianjin University, China.

Author Contributions

All authors designed the outline of the manuscript. L.Y. and W.B.M. wrote the main text; X.C.W. contributed detailed discussions and revisions; All the authors reviewed the manuscript.

Additional Information

Competing financial interests: The authors declare no competing financial interests.

How to cite this article: Yin, L. *et al.* Ferroelectric Metal in Tetragonal $BiCoO_3$/$BiFeO_3$ Bilayers and Its Electric Field Effect. *Sci. Rep.* **6**, 20591; doi: 10.1038/srep20591 (2016).